Bol. Soc. Paran. Mat.
©SPM – E-ISSN-2175-1188
SPM: www.spm.uem.br/bspm

(3s.) **v. 2026 (44) 12** : 1–19.
ISSN-0037-8712
doi:10.5269/bspm.81379

Gold Nanoparticles' Effect on MHD Blood Flow via a Stenosed Artery

S. Salgare, M. Dhange, Bhim Shinde, Kusha Chavan, Nurul Aini Jaafar and J. C. Misra

ABSTRACT: This work employs a rheological model for a theoretical investigation of stress on the walls of the artery and how the enhanced MHD flow of blood circulation through an oblique artery is affected by flow impedance resistance in gold nanoparticles. Blood is designed as a viscous fluid containing a mixture of gold nanoparticles to enhance its thermal and flow characteristics. Analytical solutions are made possible by simplification under low Reynolds number and mild stenosis circumstances. The temperature, velocity profiles, wall shear stress (WSS), and stream resistivity (FR) can all be determined using the current analytical method. In the discussion section, the results are displayed graphically. The analysis indicates that gold nanoparticles significantly reduce resistance and alter wall shear profiles, while an increasing magnetic field tends to elevate flow resistance. These findings can assist in optimizing the use of nanofluids in biomedical applications involving stenosed arteries and catheter-based therapies.

Keywords: Inclined artery, flow resistivity, oblique artery, A_u-nanoparticles, magnetic field, wall shear stress.

Contents

1. Introduction

Blood consists of plasma and various suspended particles. It is understood that red blood cells tend to accumulate near the centerline. The flow dynamics of blood within closed vessels are complex and difficult to comprehend. Furthermore, blood vessel structural abnormalities affect hemodynamics, which leads to the development of diseases like atherosclerosis. Blood consistently exhibits the characteristics of a Newtonian fluid as it passes through a tube with a suitable radius. A more accurate representation of blood flow is necessary for analysis. This knowledge can improve our methods in other domains like biophysics and medicine, enabling more accurate forecasts of blood behavior under different circumstances. According to Faharaeus- Linquist [1], blood flow in tubes smaller than 0.3 mm is not covered by the law of Poiseuille, blood viscosity decreases when blood vessel diameter decreases below 0.3 mm, and as a result, resistance to flow in arterioles also decreases. Experimental research has shown that there is an exterior layer of plasma that is cell-free and a core region that contains erythrocytes [2,3]. The findings of Hynes [4] show that when blood passes through arteries that are 1000 μm wide or less, the theory that blood is a single-phase fluid is refuted. In his research, the researcher came to the conclusion that at very low shear rates, the RBCs would be in touch with the vessel wall, and the peripheral region would not exist. These RBCs may enhance wall friction, which raises flow resistance. The peripheral layer forms when the shear rate is strong enough to lubricate suspended particles, which can lessen flow resistance in tubes with small diameters. The modified Casson fluid model and the modified Herschel-Bulkley model are used to study the behavior of blood flow in microvessels. It is discovered that the modified Herschel-Bulkley model is more complete than the modified Casson fluid model. Furthermore, the outcomes of both models are contrasted with data from the literature, which demonstrates the importance of the plasma layer in

2020 *Mathematics Subject Classification:* 92C10, 76V05, 76Z05.
Submitted January 16, 2026. Published April 21, 2026

microcirculation and the apparent Newtonian behavior of blood in microvessels when it is present [5]. Red blood cells are thought to be concentrated in the middle of the artery and nearly nonexistent close to the wall. Therefore, the only fluid present close to the artery wall is plasma. Additionally, it is known that blood viscosity varies between the vessel's core and periphery. The presence, thickness, and viscosity of the peripheral plasma layer in a two-layered fluid are important factors in changing the resistance to flow and frictional stress in diseased blood arteries [6–8]. Simulations of circulation patterns in stenosed blood vessel walls were created by Azuma-Fukushima [9]. MacDonald [10] noted the effect of vascular stenosis on continuous flow. Using a mathematical model, [11, 12] investigated the blood flow in multi stenosis and inclination with body spurt. Then, a number of studies utilizing lifeblood under various conditions, including non-Newtonian or Newtonian liquids, looked at the flow characteristics of lifeblood in a pipe with slight contraction (see [13–21]).

Researchers are currently very concerned about nanofluid for a variety of reasons. The term "nanofluid" refers to a fluid restructuring method that uses nanoscale elements with a wavelength of less than 50 nm. Nanofluids may have better thermophysical characteristics than conventional fluids. Microelectronics, fuel-cell technology, pharmaceuticals, hybrid power machines, home refrigerators, nuclear device coolants, freezing equipment, and space machineries are just a few of the many businesses that use nanofluids. Choi and Eastman [22] were the originators who made this technique widely known. Unlike other methods of drug delivery, graphene and its associated compounds in nanomedicine offer several unique benefits, including an exceptionally large surface area, high drug-loading efficiency, enhanced stability, the ability to control release rates, ease of surface modification, strong near-infrared (NIR) absorption, size customization, excellent biocompatibility, and low toxicity. Aside from its utility in biomedical fields, graphene oxide shows numerous morphological and physiological differences that can influence the heart and blood vessels. Factors such as the level of oxygen content, the size and form of the pieces, and the layer count all play a role in determining the biocompatibility of graphene oxide with various tissue types, cell types, and structures. Tunable, covalent, and noncovalent integration can improve drug transport properties by reducing negative effects and boosting graphene oxide's water dispersal, which is further impeded by its high ionic strength. Godin et al. [23] reviewed the utilization of nanoparticles for advanced therapies and molecular imaging, as well as drug-eluting stents with specific designs, and in vivo/ex vivo early detection methods. Several researchers ([24–29]) addressed the mixed blood flow of nanoparticles and showed how this method enables us to anticipate such problems and achieve the desired outcomes. Furthermore, Vajravelu et al. [30] investigated convective heat transfer in a nanofluid (NF) stream that ends in an elongating surface, concentrating on silver-water and C_u- water NFs. Along with the highest-temperature unique under the infection-dependent development of warmth within or integration and warm air endurance proficiencies, they also looked at the characteristics of the NPs' capacities element in the stream. Akbar et al. [31] provided a detailed explanation of the impacts of thermal power creation and flow in the peristalsis with small particles contacting $H_2O + C_u$. They compared the results for the natural-water foundation model and copper-water (Cu-water). Akbar [32] investigated the effects of endoscopes on a Cu-water nanofluid's (NF) peristaltic stream. Elnaqeen et al. [33] used a catheter-equipped mildly narrowed artery with thrombosis to study the Cu-blood stream model. Zaman et al. [34] investigated the effects of slip-on unstable blood flow across a curved stenosed channel using copper and silver nanoparticles. Zaman et al. [35] investigated the volatile dispersion of tiny particles in blood in a distinct investigation. The Carreau liquid model is used in the paper to explain the non-Newtonian characteristics of blood. Elnaqeeb et al. [36] used flexible viscosity to examine the hemodynamic characteristics of a blood stream containing nanoparticles of gold in a shortened artery. Mekheimer et al. [37] combined study examined how metallic nanoparticles and magnetic forces affected a micropolar fluid flowing through a stenotic artery. The sources contain studies conducted by various researchers on additional uses of nanoparticles (NPS) that are utilized in blood physiology [38–41].

Arterial stenosis can cause major problems and disrupt the normal operations of the heart and lungs. Specifically, it may result in aberrant cell proliferation in the stenotic area, an increased chance of full blockage, and a jump in resistance to circulation that might significantly reduce blood flow. Nonetheless, a number of investigators have employed suspended nanoparticles to examine how different forms of stenosis impact the circulatory system ([42–50]). The thermophysical properties of gold nanoparticles (NPs), water, and blood are shown in Table 1

The current study examines the unique impacts of a force field on bloodstream flow using gold nanoparticles and water as the basic fluid, drawing inspiration from earlier research. According to Figure 1, this fluid appears to pass through a stenosed artery that is sloping over it. We examine stream resistance, the shear stress, and pressure droplet on the boundary, and the facts illustrate the clear consequences of a number of significant constraints. The theoretical and physical replicas are explained in part 2, and the results are discussed in part 3.

2. Formulation of the Issue and its Resolution

Analyze how a sticky, incompressible liquid moves through a tube with a unvarying cross-section and an oblique axisymmetric manifold. The stenosis should be modest and increase correspondingly in the axial direction. Figure 1 depicts the surface shape.

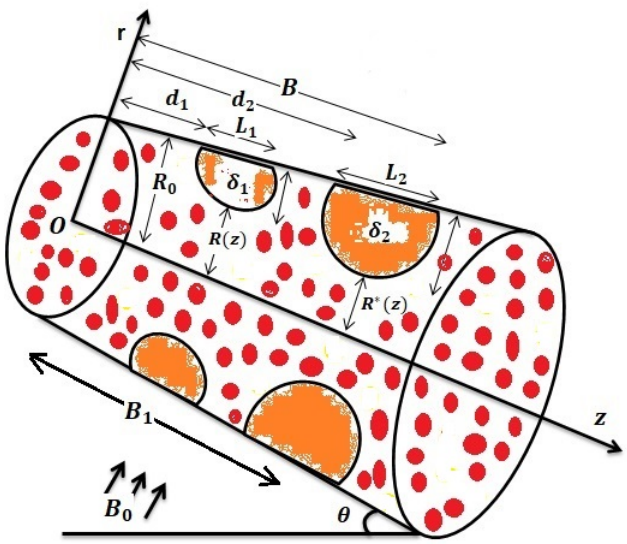

Figure 1: Design of multiple stenosis.

The formula pertaining to the wall's geometry is (Prasad Radhakrishnamacharya [12]).

$$h(z) = \begin{cases} R_0, & 0 \le z \le d_1 \\ R_0 - \frac{\delta_1}{2}\left(1 + \cos\frac{2\pi}{L_1}\left(z - d_1 - \frac{L_1}{2}\right)\right), & d_1 \le z \le d_1 + L_1 \\ R_0, & d_1 + L_1 \le z \le B_1 - \frac{L_2}{2} \\ R_0 - \frac{\delta_1}{2}\left(1 + \cos\frac{2\pi}{L_2}(z - B_1)\right), & B_1 - \frac{L_2}{2} \le z \le B_1 \\ R^*(z) - \frac{\delta_2}{2}\left(1 + \cos\frac{2\pi}{L_2}(z - B_1)\right), & B_1 \le z \le B_1 + \dfrac{L_2}{2} \\ R^*(z), & B_1 + \frac{L_2}{2} \le z \le B. \end{cases} \tag{2.1}$$

Here B is the channel's length, L_1, and L_2 are the lengths, and δ_1 is the primary and δ_2 secondary stenosis's maximum heights, respectively.

2.1. Principal Mathematical Formula

According to this interpretation, blood is a consistent, non-Newtonian, and incompressible fluid. Its viscosity can be described using a range of non-Newtonian fluid models, including the power-law, Herschel-Bulkley, micropolar, and other fluid models. In contrast to other sticky prototypes, this viscous liquid paradigmatic accurately captures the viscous nature characteristic of biological blood in daily life, we used it to explain the physical substance of blood in our work (Pratumwal et al. [45]).

According to Akbar-Butt [39], the flow for the current circumstance is crucially articulated as follows:

$$\frac{\partial w}{\partial z}+\frac{v}{r}+\frac{\partial v}{\partial r}=0, \tag{2.2}$$

$$\rho_{nf}\left(v\frac{\partial v}{\partial r}+w\frac{\partial v}{\partial z}\right)=-\frac{\partial p}{\partial r}+\mu_{nf}\frac{\partial}{\partial r}\left(2\frac{\partial v}{\partial r}\right)+\mu_{nf}\frac{\partial}{\partial z}\left(2\frac{\partial v}{\partial z}+\frac{\partial w}{\partial r}\right)-\rho_{nf}g\cos\theta, \tag{2.3}$$

$$\rho_{nf}\left(v\frac{\partial w}{\partial r}+w\frac{\partial w}{\partial z}\right)=-\frac{\partial p}{\partial z}+\mu_{nf}\frac{\partial}{\partial z}\left(2\frac{\partial w}{\partial z}\right)+\frac{\mu_{nf}}{r}\frac{\partial}{\partial r}\left[r\left(\frac{\partial v}{\partial z}+\frac{\partial w}{\partial r}\right)\right]-g\rho_{nf}\alpha(T-T_0)-\sigma B_0^2 w+\rho_{nf}g\sin\theta, \tag{2.4}$$

$$v\frac{\partial T}{\partial r}+w\frac{\partial T}{\partial z}=\frac{k_{nf}}{(\rho c_p)_{nf}}\left(\frac{\partial^2 T}{\partial r^2}+\frac{1}{r}\frac{\partial T}{\partial r}+\frac{\partial^2 T}{\partial z^2}\right)+\frac{Q_0}{(\rho c_p)_{nf}}. \tag{2.5}$$

2.2. Borderline Conditions (BC) and Theoretical Solution

Threshold limits are essential for calculating the resolutions to replicated physical problems. Since lifeblood components cling to the inner surface of the arterial piece under examination, it may be inferred that the longitudinal velocity (w) of lifeblood rudiments on the surface relates to a single-dimensional flow and is equivalent to the rapidity of arterial membrane stuff. .
This stenosed ingredient can be quantitatively explained as follows:

$$\text{At } r=0, \quad \left.\frac{\partial T}{\partial r}\right|_{r=0}=0, \quad \left.\frac{\partial w}{\partial r}\right|_{r=0}=0; \tag{2.6}$$

$$\text{at } r=h, \quad T=0, \quad w=0. \tag{2.7}$$

The fluid's hotness is represented by T, the element that generates or absorbs heat by Q_0, and the speed of its elements in the (r,z) coordinates by (w,v), correspondingly.

The following are the identified parameters for the nanofluids' active thermal conductivity (K_{nf}), active dynamic viscosity (μ_{nf}), heat capacitance $(\rho c_p)_{nf}$, active density (ρ_{nf}), thermal diffusivity (α_{nf}), and in that order ([30,36]):

$$\rho_{nf}=(1-\phi)\rho_f+\phi\rho_p; \qquad k_{nf}=k_f\left(\frac{k_s+2k_f-2\phi(k_f-k_s)}{k_s+2k_f+2\phi(k_f-k_s)}\right) \qquad \mu_{nf}=\frac{\mu_f}{(1-\phi)^{2.5}};$$

$$(\rho c_p)_{nf}=(1-\phi)(\rho c_p)_f+\phi(\rho c_p)_p; \qquad \alpha_{nf}=\frac{k_{nf}}{(\rho c_p)_{nf}}$$

The following dimensionless quantities were employed:

$$\bar{r}=\tfrac{r}{R_0}, \quad \bar{z}=\frac{z}{L_0}, \quad \bar{w}=\frac{w}{W}, \quad \bar{u}=\frac{L_0}{\delta W}u, \quad \bar{d_1}=\frac{d_1}{B}, \quad \bar{d_2}=\frac{d_2}{B}, \quad \bar{R}=\frac{R}{R_0}, \quad \bar{p}=\frac{WL_0\mu_f}{R_0^2}\,p.$$

$$\bar{\delta}_1=\frac{\delta_1}{R_0},\ \bar{\delta}_2=\frac{\delta_2}{R_0},\ M^2=\frac{\sigma B_0^2R_0^2}{\mu_f},\ G_r=\frac{g\alpha R_0^2T_0\rho_{nf}}{W\mu_f},\ F=\frac{\mu_{nf}c}{\rho_{nf}gR_0^2},\ \Theta=\frac{T-T_0}{T_0},\ \beta=\frac{Q_0R_0^2}{k_fT_0}. \tag{2.8}$$

Here, c represents the average velocity across the tube section's radius R_0.
Applying the previously indicated scaled variables of Eq. (2.2) in Eqs. (2.3)–(2.5) with significant stenosis $(\delta/R_0\ll 1)$ condition $\epsilon=R_0/L_0=o(1)$ yields the following after the dashes are removed.

$$\frac{\partial p}{\partial r}=-\frac{\cos\theta}{F}, \tag{2.9}$$

$$\frac{\partial p}{\partial z}=\frac{1}{(1-\varphi)^{2.5}}\frac{1}{r}\frac{\partial}{\partial r}\left(r\frac{\partial w}{\partial r}\right)-M^2w+G_r\,\Theta+\frac{\sin\theta}{F}, \tag{2.10}$$

$$\frac{1}{r}\frac{\partial}{\partial r}\left(r\frac{\partial\theta}{\partial r}\right)+\beta\left(\frac{k_{nf}}{k_f}\right)=0 \tag{2.11}$$

Using scaling factors, the artery wall must have the following temperature and velocity border conditions:

$$\text{At } r=0, \quad \left.\frac{\partial w}{\partial r}\right|_{r=0}=0, \quad \left.\frac{\partial \Theta}{\partial r}\right|_{r=0}=0; \tag{2.12}$$

$$\text{At } r=h, \quad w=0, \quad \Theta=0. \tag{2.13}$$

where Θ is the temperature, β is the quantity of heat absorption constraint, G_r is the Grashof number, and M is the attractive forced field constraint.

Using the constraint for mild stenosis and handle eq. (2.10) and Eq. (2.11) within the boundary limits Eq.(2.12) and Eq.(2.13), the fluid's velocity is calculated as follows:

$$\begin{aligned} w=&-\frac{G_r\,\beta}{4M^2}\left(\frac{k_f}{k_{nf}}\right)\left(r^2-h^2\right)-\frac{1}{M^2}\frac{\partial p}{\partial z}+\left[\frac{\frac{1}{M^2}\frac{dp}{dz}-\frac{G_r\,\beta}{M^2}\left(\frac{k_f}{k_{nf}}\right)-\frac{\sin\theta}{M^2F}}{I_0\left(Mh\sqrt{(1-\varphi)^{2.5}}\right)}\right]I_0\left(Mr\sqrt{(1-\varphi)^{2.5}}\right)\\ &+\frac{G_r\,\beta}{M^2}\left(\frac{k_f}{k_{nf}}\right)-\frac{\sin\theta}{M^2F}. \end{aligned} \tag{2.14}$$

$$\Theta=-\frac{\beta}{4}\left(\frac{k_f}{k_{nf}}\right)\left(r^2-h^2\right). \tag{2.15}$$

Some of the significant physical dimensions are listed beneath. The following is the flow rate q:

$$q=2\int_0^h r\,w\,dr. \tag{2.16}$$

This gives to us:

$$\begin{aligned} \frac{\partial p}{\partial z}=&\frac{q-\frac{G_r\,\beta\,h^4}{16M^2}\left(\frac{k_f}{k_{nf}}\right)-\frac{G_r\,\beta\,h^2}{2M^2}\left(\frac{k_f}{k_{nf}}\right)-\frac{G_r\,\beta\,h}{M^2}\left(\frac{k_f}{k_{nf}}\right)\left(\frac{I_1\left(Mh\sqrt{(1-\phi)^{2.5}}\right)}{I_0\left(Mh\sqrt{(1-\phi)^{2.5}}\right)\sqrt{(1-\phi)^{2.5}}}\right)}{-\frac{h^2}{2M^2}+\frac{h}{M^3}\left(\frac{I_1\left(Mh\sqrt{(1-\phi)^{2.5}}\right)}{I_0\left(Mh\sqrt{(1-\phi)^{2.5}}\right)\sqrt{(1-\phi)^{2.5}}}\right)}\\ &+\frac{\frac{h\sin\theta}{M^2F}\left(\frac{I_1\left(Mh\sqrt{(1-\phi)^{2.5}}\right)}{I_0\left(Mh\sqrt{(1-\phi)^{2.5}}\right)\sqrt{(1-\phi)^{2.5}}}\right)+\frac{h^2\sin\theta}{M^2F}}{-\frac{h^2}{2M^2}+\frac{h}{M^3}\left(\frac{I_1\left(Mh\sqrt{(1-\phi)^{2.5}}\right)}{I_0\left(Mh\sqrt{(1-\phi)^{2.5}}\right)\sqrt{(1-\phi)^{2.5}}}\right)} \end{aligned} \tag{2.17}$$

The following formula provides the pressure drops throughout just one wavelength $p(0)-p(\lambda)$:

$$\Delta p=-\int_0^1\frac{\partial p}{\partial z}\,dz. \tag{2.18}$$

The impedance, represented by λ, is described as follows:

$$\lambda=\frac{\Delta p}{q}. \tag{2.19}$$

Since there is no stricture ($h=1$), the purposeful pressure reduction that follows is implemented:

$$\Delta p_n=\left[-\int_0^1\frac{\partial p}{\partial z}\,dz\right]\Bigg|_{h=1}. \tag{2.20}$$

The amount of resistance in a usual artery can be found using the following technique:

$$\lambda_n=\frac{\Delta p_n}{q}. \tag{2.21}$$

The standardized resistance of a stream can be written as follows:

$$\bar{\lambda} = \frac{\lambda}{\lambda_n}. \tag{2.22}$$

Shear stress in the blood vessel wall is one of the physical factors that greatly influences the liquid flow at the barrier. The succeeding formulary can be utilized to compute the wall shear stress:

$$\bar{\tau}_w = -\frac{h}{2}\frac{\partial p}{\partial z}. \tag{2.23}$$

Table 1: Thermophysical properties of the nanoparticles (A_u), water, and blood (see [44])

Physical Properties	Blood	A_u(Gold)	Fluid Phase
C_p(J/Kg K)	3594	128.8	4179
ρ(Kg/m^3)	1063	19320	997.1
K(W/m K)	0.492	314.4	0.613
$\gamma \times 10^{-5}$ (K^{-1})	0.18	1.4×10^{-5}	21.0

3. Computational Findings and Discussion

The accuracy of the analytical equations Eqs. (2.14, 2.15, 2.22, 2.23) has been tested in this study using suitable numerical computations. MATHEMATICA software was used to analyze the effects of different limitations. The whole set of results is shown in Figures 2–27. In figures, pure blood is represented by the colour red ($\phi = 0$), and A_u-blood by the colour blue ($\phi \neq 0$).

The wall shear-stress (WSS) $\bar{\tau}_w$ against the axial length (z) is shown in Figs. 2–8 for a range of heat absorption constant (β), Grashof number (G_r), stenosis heights (δ_1, δ_2), angle of bent (θ), field of attractive force constraint (M), and flow rate (q) values. It is concluded from these figures that the magnitude of WSS increases as blood flows in the stenotic region, it gets its maximum at the peak of stenosis at $z = 0.7$, and it gradually decreases when the severity of stenosis declines. The same behavior is observed in [44, 46]. The oscillation is more noticeable in the presence of A_u particles in the blood than in pure blood. Figure 3 illustrates that the magnitude of wall shear stress rises with increasing Grashof number. A higher Grashof number, which measures the ratio of buoyancy to viscous forces, signifies enhanced buoyancy effects. These buoyancy forces enhance natural convection, which in turn increases the velocity gradient near the arterial wall. Therefore, wall shear stress rises. The same behavior is obtained by absorption constant, force field constraint, volumetric flow rate, rate of inclination, and severity of stenosis as presented in figures (Figs. 2, 4–8). This finding is consistent with the result reported in Elnaqeeb [44].

The connection between stenosis height and flow resistance (FR) for numerous values of the Grashof number (G_r), attractive force field constraint (M), absorption of heat constant (β), flow rate (q), and the angle of the bent (θ) is shown in Figures 9–18. Under all limitations, it is evident that the FR increases in proportion to the narrowing heights (δ_1, δ_2). Nevertheless, Figs. 9 and 10 show that it falls as the heat absorbance constant (β) increases. The physical foundation of this finding should be noted. Because the restricted fluid in the constricted region moves quickly into the main flow region, the fluid briefly boosts its resistance to flow in the pre-stenotic zone prior to attaining its lowest level in the post-stenotic region. Furthermore, it is seen that FR decreases with increases in the attractive force field constraint (M), angle of bent (θ), Grashof number (G_r), and flow rate (q) (see Figs. 11–18), but flow resistivity upsurges with an upsurge in q (see Figs. 17–18). When there is a decrease in the resistance to flow brought on by an increase in fluid velocity, brought on by an elevation in volume flow rate, an angle of oblique, and strong buoyant forces, blood can pass through arteries with ease. Additionally, A_u-blood is shown to flow less

readily than pure blood. This is due to the fact that gold increases the flexibility of arteries. These findings are consistent with Elnaqeeb's [36].

Here, Figs. 19–21 illustrate the relationship between temperature (θ) and radial distance (r) over a range of narrowing heights (δ_1, δ_2), and the source of heat or sinking constraint (β). The temperature rises as the heat-absorbing constant increases, while it decreases when the narrowing height grows. Further observation is that pure blood alters temperature more quickly than A_u-blood. These results corroborate those of Akabar [41].

The speed variation throughout the radial axis is depicted in Figures 22–27 for a range of the narrowing heights (δ_1, δ_2), attractive force field constraint (M), Grashf number (G_r), and angle of bent (θ), and heat absorption constant (β). Figure 22 illustrates how speed increases as the hheat-absorbingconstant (β) increases. The blood becomes thinner and moves through arteries faster as the heat-absorbing constant increases, increasing the velocity. Fluid speed decreases as the force constant (M) grows while it increases as the Grashof number (G_r) increases (see Figs. 23, 24). Strong electromagnetic and buoyancy electromagnetic forces comparative to sticky forces can lower the velocity field, causing blood to flow more slowly in arteries. Figure 25 shows how the fluid's speed declines as the slant angle (θ) surges. Blood moves through arteries more slowly as stenosis height rises, reducing speed (Figs. 26–27). Because gold makes arteries more flexible, which lowers the flow rate, pure blood is also shown to have a faster velocity than A_u-blood. These findings align with the results as reported in [36, 41].

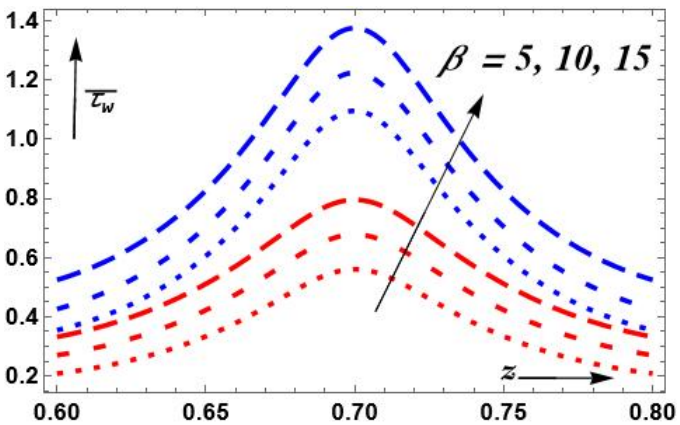

Figure 2: Design of β and z on $\bar{\tau}_w$

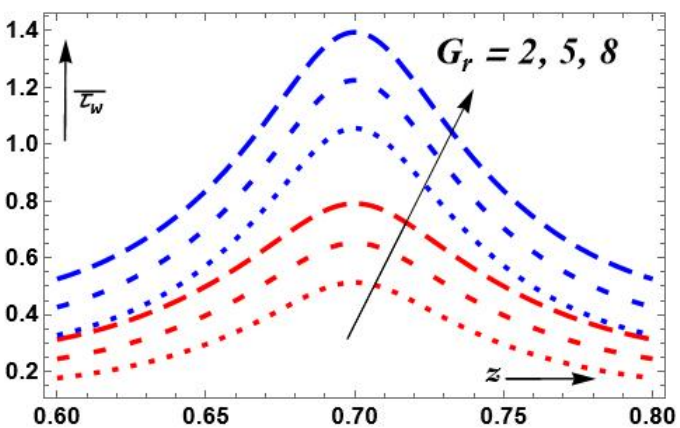

Figure 3: Design of G_r and z on $\bar{\tau}_w$

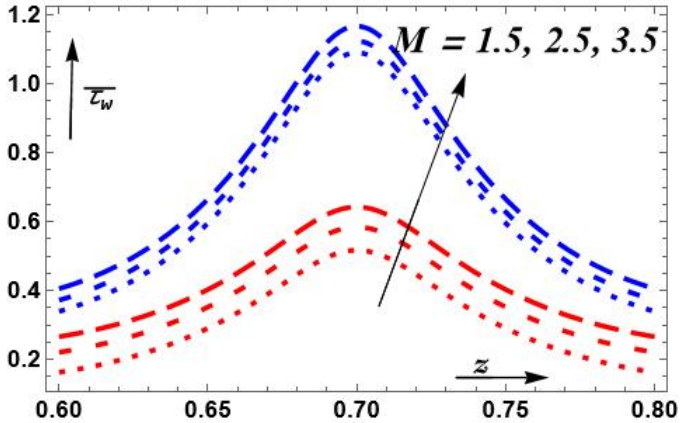

Figure 4: Design of M and z on $\bar{\tau}_w$

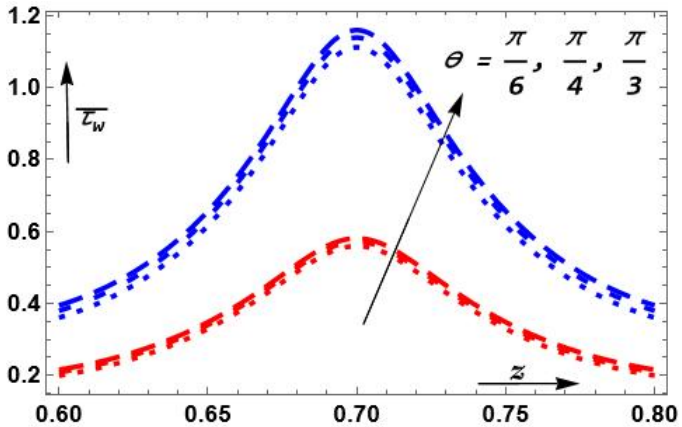

Figure 5: Design of θ and z on $\bar{\tau}_w$

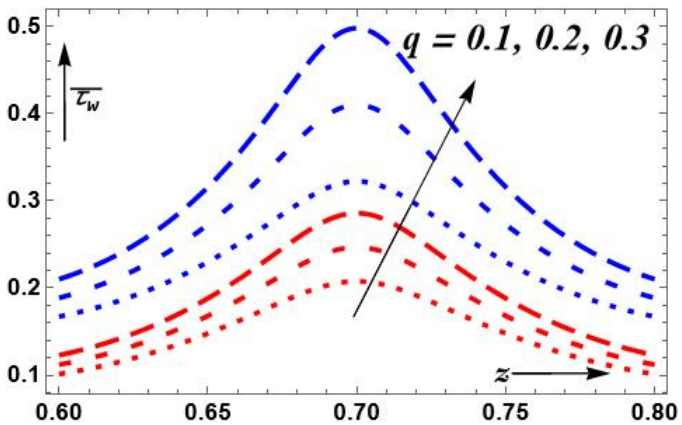

Figure 6: Design of q and z on $\bar{\tau}_w$

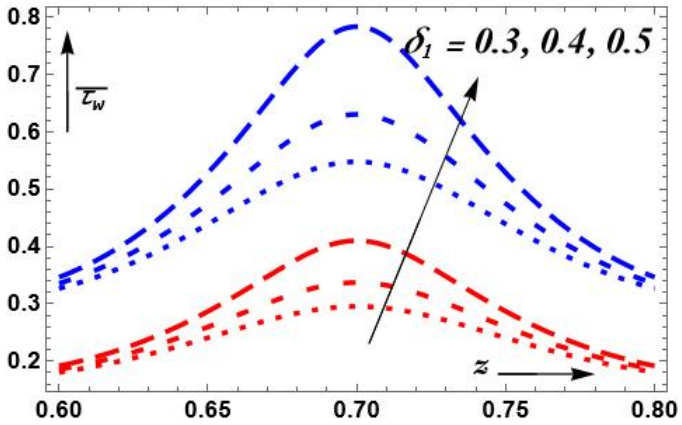

Figure 7: Design of δ_1 and z on $\bar{\tau}_w$

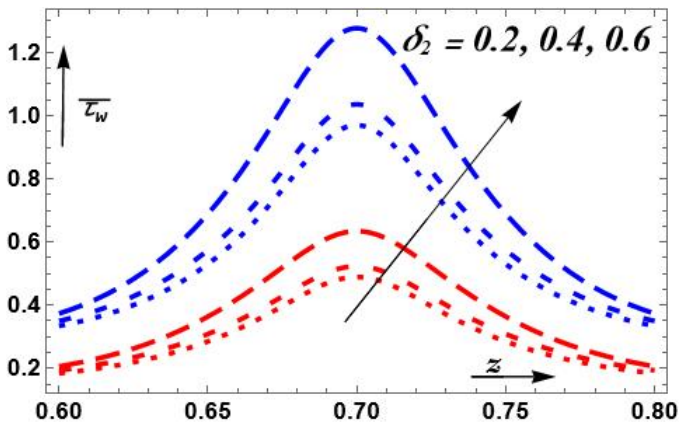

Figure 8: Design of δ_2 and z on $\bar{\tau}_w$

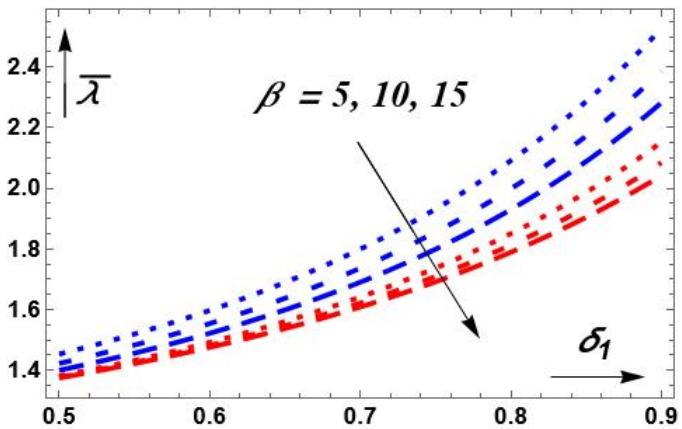

Figure 9: Design of β and δ_1 on $\bar{\lambda}$

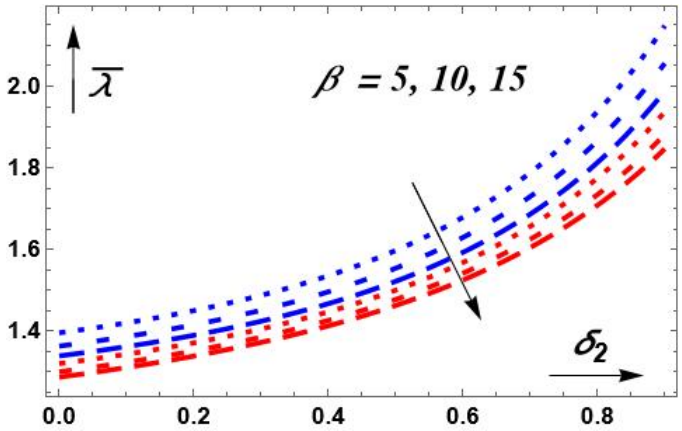

Figure 10: Design of β and δ_2 on $\bar{\lambda}$

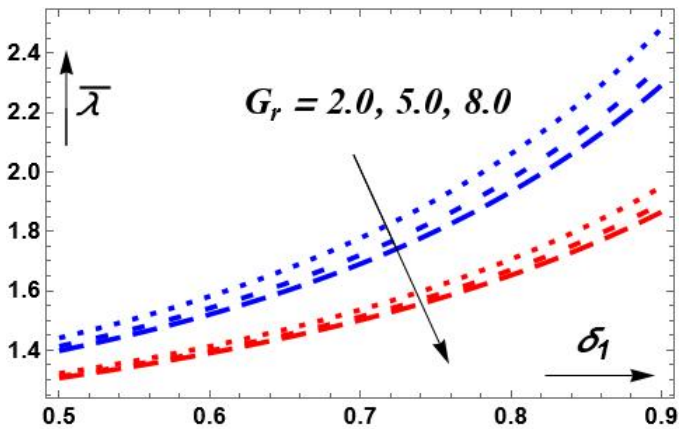

Figure 11: Design of G_r and δ_1 on $\bar{\lambda}$

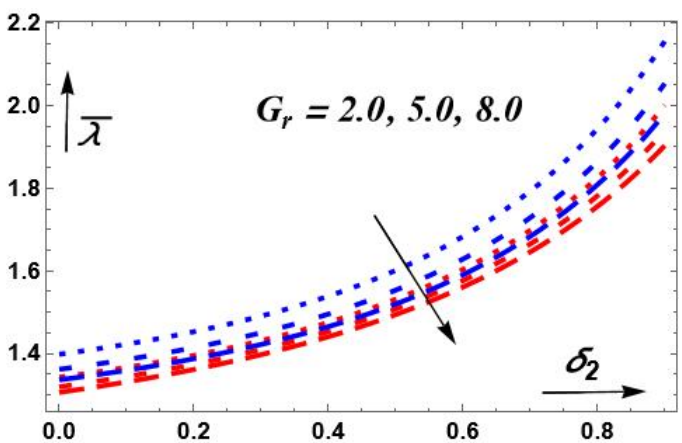

Figure 12: Design of G_r and δ_2 on $\bar{\lambda}$

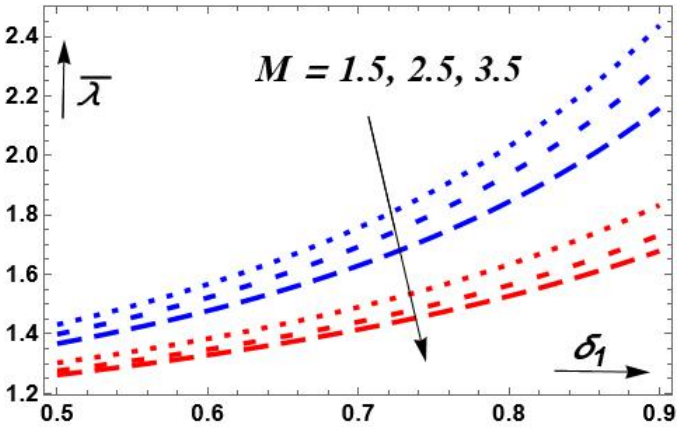

Figure 13: Design of M and δ_1 on $\bar{\lambda}$

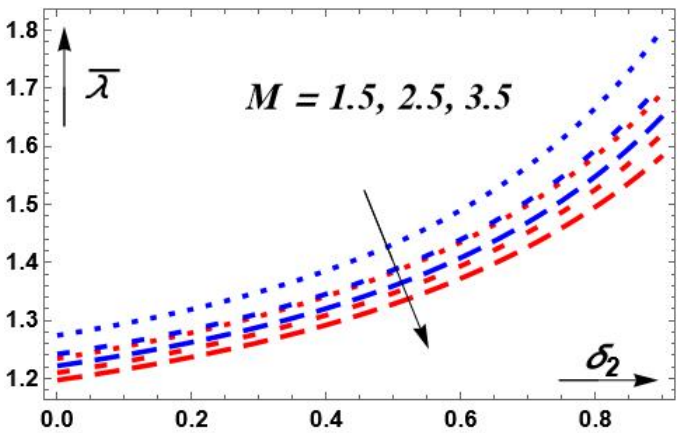

Figure 14: Design of M and δ_2 on $\bar{\lambda}$

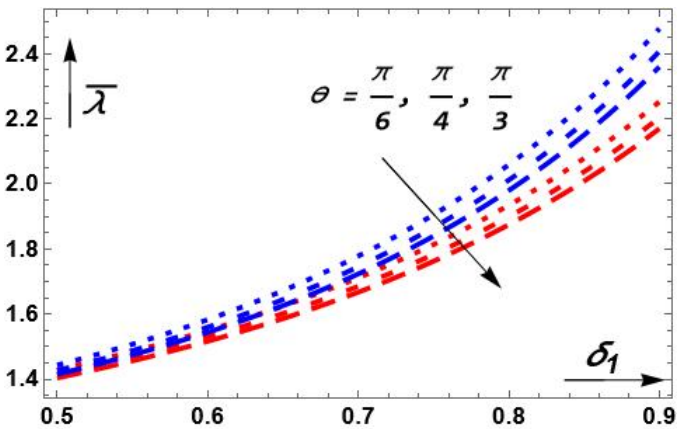

Figure 15: Design of θ and δ_1 on $\bar{\lambda}$

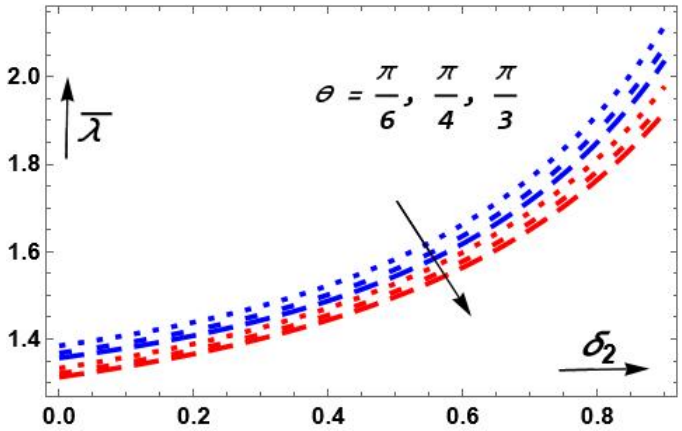

Figure 16: Design of θ and δ_2 on $\bar{\lambda}$

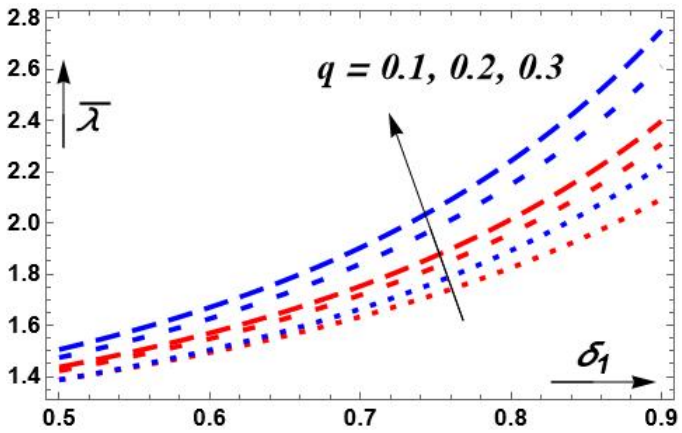

Figure 17: Design of q and δ_1 on $\bar{\lambda}$

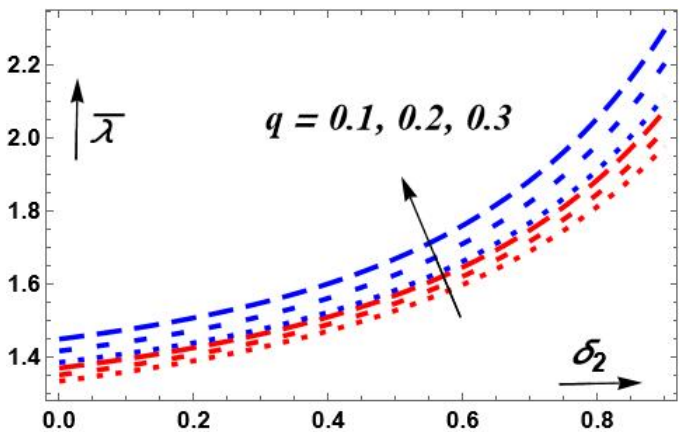

Figure 18: Design of q and δ_2 on $\bar{\lambda}$

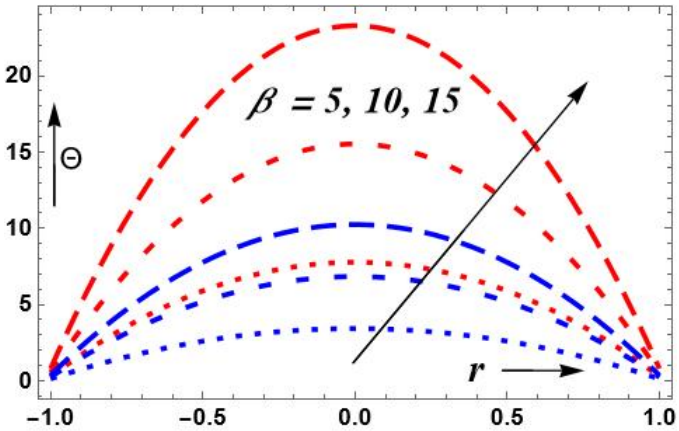

Figure 19: Design of β and r on Θ

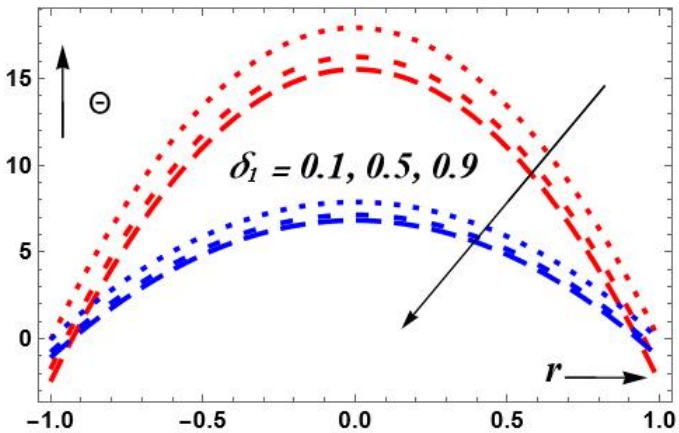

Figure 20: Design of δ_1 and r on Θ

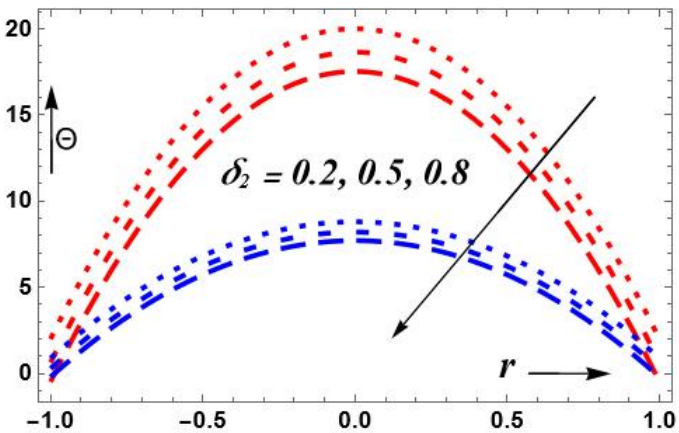

Figure 21: Design of δ_2 and r on Θ

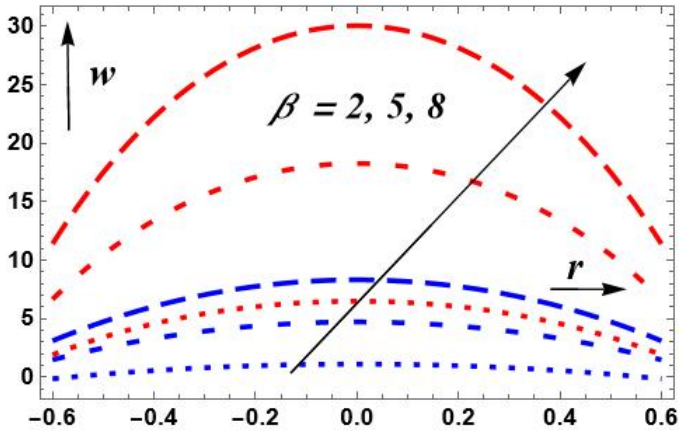

Figure 22: Design of β and r on w

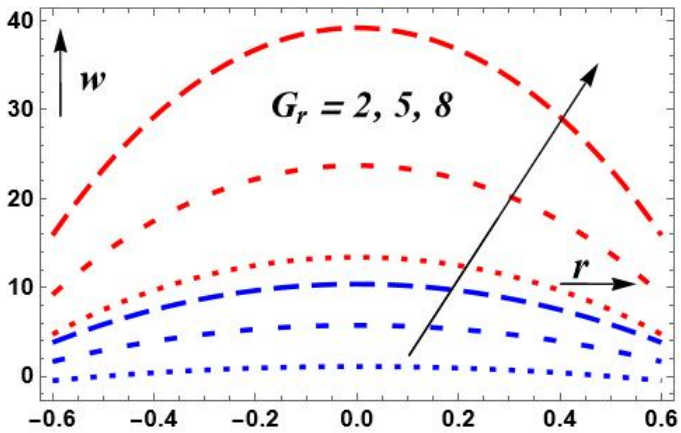

Figure 23: Design of G_r and r on w

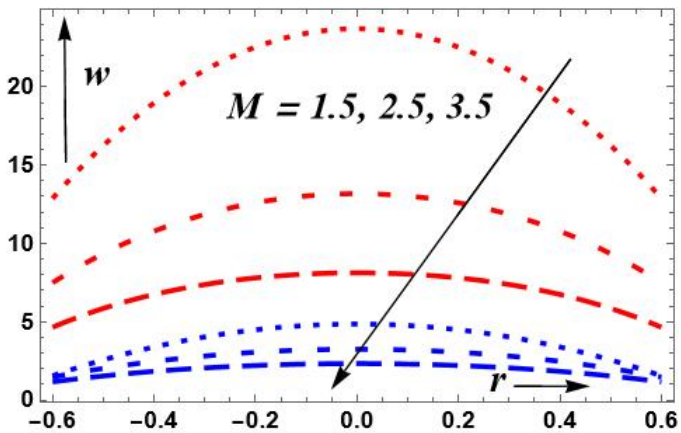

Figure 24: Design of M and r on w

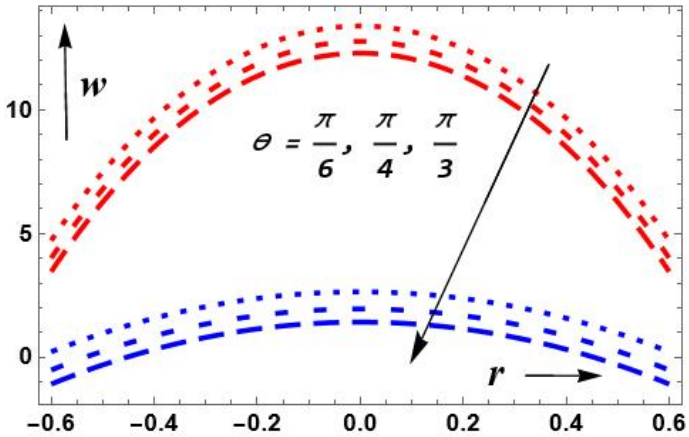

Figure 25: Design of θ and r on w

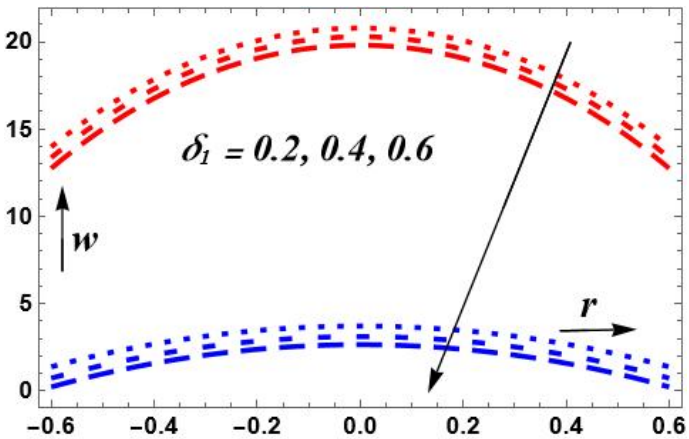

Figure 26: Design of δ_1 and r on w

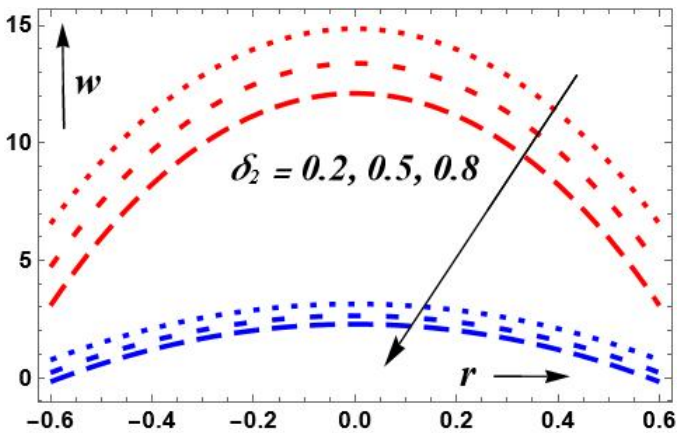

Figure 27: Design of δ_2 and r on w

4. Concluding Remarks

In this theoretical investigation, we examine the flow of blood containing A_u-nanoparticles through a slanted artery. The combined effects of immense magnetic forces are necessary for the study of flow dynamics. The current mathematical model uses water as the base liquid and A_u nano-particles to examine how an attractive forced field impacts lifeblood circulation through an oblique manifold stenosed conduit. The outcomes for different slanted angles, radial distance, altitude of stenosis, and expansion following stenosis values are shown graphically. The following are the key conclusions:

- Due to the fact that gold makes arteries more elastic, A_u-blood has a higher flow resistance than pure blood.
- For all constraints, the speed of a fluid is greater in pure blood than in A_u- blood.
- The flow resistance upsurges with increasing volume flow rate but declines with increasing Grashof number, attractive force field constraint, heat absorption constraint, and slanted angle.
- The fluid's speed decreases due to higher buoyant and electro-magnetic forces in comparison to viscous forces.
- The Grashof number, absorption of heat constraint, force field limitation, narrowing height, angle of proclivity, and volume flow rate all contribute to an increase in wall shear stress.
- When the stenosis height increases, the fluid's temperature decreases, but it increases when the heat-absorbing constant is increased. The regions nearest the outermost walls possess the lowest temperature, whereas the center of the tube has the highest.

References

1. R. Fahraeus, T. Lindqvist, *The viscosity of the blood in narrow capillary tubes.* Am. J. Physiol.-Legacy Content., 96 (1931), no. 3, 562-570. https://doi.org/10.1152/ajplegacy.1931.96.3.562
2. G. Bugliarello, J. Sevilla, *Velocity distribution and other characteristics of steady and pulsatile blood flow in fine glass tubes.* Biorheol., 7 (1970), no. 2, 85-107. https://doi.org/10.3233/BIR-1970-7202.
3. G. R. Cokelet, *The rheology of human blood* (Doctoral dissertation, Massachusetts Institute of Technology), 1963.
4. R. H. Haynes, *Physical basis of the dependence of blood viscosity on tube radius.* Am. J. Physiol.-Legacy Content., 198 (1960), no.6, 193-200. https://doi.org/10.1152/ajplegacy.1960.198.6.1193
5. N. Iida, *Influence of plasma layer on steady blood flow in microvessels.* Japanese J. Appl. Phy., 17 (1978), 1, 203. https://doi.org/10.1143/JJAP.17.203
6. J. B. Shukla, R. S. Parihar, S. P. Gupta, S.P. *Effects of peripheral layer viscosity on blood flow through the artery with mild stenosis.* Bull. Math. Biol., 42 (1980), 797-805. https://doi.org/10.1007/BF02461059
7. V. P. Srivastava, M. Saxena, *Two-layered model of Casson fluid flow through stenotic blood vessels: applications to the cardiovascular system.* J. Biomech., 27 (1994), no.7, 921-929. https://doi.org/10.1016/0021-9290(94)90264-X
8. D. F. Young, *Effect of a time dependent stenosis of flow through a tube.* J. Eng. Indust. Trans. ASME., 90 (1968), 248-254.
9. T. Azuma, T. Fukushima, *Flow patterns in stenotic blood vessel models.* Biorheol., 13 (1976), 337-355.
10. D. A. Macdonald, *On Steady flow through modelled vascular stenosis.* J. Biomech. 12 (1979), 13-30.
11. N. Verma, R. S. Parihar, *Effect of magneto-hydrodynamics and haematocrit on blood flow in an artery with multiple mild stenosis.* Int. J. Appl. Math. Comput., 1 (2009), no.1, 30-46.
12. K. M. Prasad, G. Radhakrishnamacharya, *Flow of Herschel-Bulkley fluid through an inclined tube of non-uniform cross-section with multiple stenoses.* Arch. Mech., 60 (2008), 161-172.
13. J. H. Forrester, D. F. Young, *Flow through a conversing diverging tube and its implications in occlusive vascular disease.* J. Biomech., 3 (1970), 297-316.
14. J. Perkkio, R. Keskinen, *The effect of the concentration profile of red cells on blood flow in the artery with stenosis.* Bull. Math. Biol., 45 (1983), no.2, 259-267.
15. J. C. Misra, B. K. Kar, *Momentum integral method for studying flow characteristics of blood through a stenosed vessel.* Biorheol., 26 (1989), 23-35.

16. P. N. Tandon, U. V. Rana, M. Kawahara, V. K. Katiyar, *A model for blood flow through stenotic tube.* Int. J. Biomed. Comput., 32 (1993), .62-78.

17. M. Nakamura, T. Sawada, *Numerical study on the flow of a non-Newtonian fluid through an axisymmetric stenosis.* J. Biomech. Eng., 110 (1988), 137-143.

18. M. K. Sharma P. R. Sharma, V. Nasha, *Pulsatile MHD arterial blood flow in the presence of double stenosis.* J. Appl. Fluid Mech., 6 (2013), no.3, 331-338.

19. A. K. Gupta, G. D. Gupta, *Unsteady blood flow in an artery through a non-symmetrical stenosis.* Acta Ciencia Indica. XXVII M, 2 (2001), 137-142.

20. R. N. Pralhad, D. H. Schultz, *Modelling of arterial stenosis and its applications to Blood diseases.* Math. Biosci., 190 (2004), 203-220.

21. R. Ponalagusamy, *Two-fluid model for blood flow through a tapered arterial stenosis: Effect of non-zero couple stress boundary condition at the Interface.* Int. J. Comput. Math. 3 (2017), no. D, 807- 824.

22. S. U. S. Choi, J. A. Eastman, *Enhancing thermal conductivity of fluids with nanofluids.* ASME Fluids Engg. Div. 231 (1995), 99-105.

23. B. Godin, J. H. Sakamoto, R. E. Serda, A. Grattoni, A. Bouamrani, A. M. Ferrari, *Emerging of nano-medicine for the diagnosis and treatment of cardio-vascular diseases.* Trends. Pharmacological Sci., 31 (2010), 199-205.

24. J. Buongiorno, *Convective transport in nanofluids.* J. Heat Trans. 128 (2006), no.3, 240-250. http://dx.doi.org/10.1115/1.2150834

25. . S. Akbar, Z. , *Metachronal beating of cilia under the influence of Casson fluid and magnetic field.* J. Magn. Magn. Mater., 378 (2015), 320-326.

26. K. M. Prasad, N. Subadra, S. K. Reddy, *Peristaltic transport of a couple stress fluid with nanoparticles having permeable walls.* J. Nanofluids., 6 (2017), 751-760.

27. A. Rahbari, M. Fakour, A. Hamzehnezhad, M. A. Vakilabadi, D. D. Ganji , *Heat transfer and fluid flow of blood with nanoparticles through porous vessels in a magnetic field: A quasi-one-dimensional analytical approach.* Math. Biosc.,283 (2017), 38-47.

28. M. D. Hatami, D. D. Ganji, *Computer simulation of MHD blood conveying gold nanoparticles as a third grade non-Newtonian nanofluid in a hollow porous vessel.* Comput. Meth. Prog. Bio., 113 (2014), no.2, 632-641.

29. K. S. Mekheimer, E. L. Elnaqeeb, M. A. Kot, F. Alghamdi, *Simultaneous effect of magnetic field and metallic nanoparticles on a micropolar fluid through an overlapping stenotic artery: Blood flow model.* Phys. Essays., 29 (2016), no. 2, .272-283. https://doi.org/10.4006/0836-1398-29.2.272

30. K. Vajravelu, K. V. Prasad, J. Lee, C. Lee, I. Pop, R. A. V. Gorder, *Convective heat transfer in the flow of viscous Ag-water and Cu-water nanofluids over a stretching surface.* Int. J. Therm. Sci., 50 (2011), 843.

31. N. S. Akbar, M. Raza, M. R. Ellahi, *Influence of heat generation and heat flux in peristalsis with interaction of nanoparticles.* European Phys. J. Plus., 129 (2014), 185.

32. N. S. Akbar, *Endoscope effects on the peristaltic flow of Cu-water nanofluids.* J. Comut. Theor. Nanosci., 11 (2014), 1150-1155.

33. T. Elnaqeeb, K. S. Mekheimer, F. Alghamdi, *Cu-blood flow model through a catheterized mild stenotic artery with a thrombosis.* Math. Biosci., 282 (2016), 135-146.

34. A. Zaman, N. Ali, I. Ali, *Effects of nanoparticles (Cu, Ag) and slip on unsteady blood flow through a curved stenosed channel with aneurysm.* Thermal. Sci. Eng. Prog., 5 (2018), 482-491.

35. A. Zaman, A. A. Khan, N. Ali, *Modelling of unsteady non-Newtonian blood flow through a stenosed artery with nanoparticles.* J. Brazilian Soc. Mech. Sci. Eng., 40 (2018), 307. https://doi.org/10.1007/s40430-018-1230-5

36. T. Elnaqeeb, N. A. Shah, K. S. Mekheimer, *Hemodynamic characteristic of gold nanoparticle blood flow through a tapered stenosed vessel with variable nanofluid viscosity.* Bio. Nano. Sci. 9 (2019), 245-255. https://doi.org/10.1007/s12668-018-0593-5

37. K. S. Mekheimer, T. Elnaqeeb, M. A. El-Kot, F. Alghamdi, *Simultaneous effect of magnetic filed and metallic nanoparticles on a micropolar fluid through an overlapping stenotic artery: Blood flow model.* Phy. Essays., 29 (2016), no. 2, 272-283.

38. S. Nadeem, S. Ijaz, *Nanoparticles analysis on the blood flow through a tapered catheterized elastic artery with overlapping stenosis.* Eur. Phys. J. Plus., 129 (2014), no.11, 249.

39. N. S. Akbar, A. W. Butt, *Magnetic field effects for copper suspended nanofluid venture through composite stenosed arteries with permeable walls.* J. Magn. Magn. Mater., 381 (2015), 285-291.

40. A. Zaman, N. Ali, N. Kousar, *Nanoparticles (Cu, TiO2, Al2O3) analysis on unsteady blood flow through an artery with a combination of stenosis and aneurysm.* Compt. Math. Appl., 76 (2018), no.9, 2179-2191. https://doi.org/10.1016/j.camwa.2018.08.019

41. N. S. Akbar, *Metalic nanoparticle analysis for the blood Flow in tapered stenosed arteries: Application in nanomedicines.* Int. J. Bio. Math., 9 (2016), no.1, 1-18. https://doi.org/10.1142/S1793524516500029

42. B. C. Pak, Y. I. Cho, *Hydrodynamic and heat transfer study of dispersed fluids with submicron metallic oxide particles.* Exp. Heat Transf., 11 (1998), no.2, 151-170.

43. K. S. Mekheimer, M. S. Mohamed, T. Elnaqeeb, *Metallic nanoparticles influence on blood flow through a stenotic artery.* Int. J. Pure. Appl. Math. 107 (2016), no. 1, 201-220.

44. T. Elnaqeeb, *Modeling of A_u (NPs)-blood flow through a catheterized multiple stenosed artery under radial magnetic field.* Eur. Phys. J. 228 (2019), 2695-2712. https://doi.org/10.1140/epjst/e2019-900059-9

45. Y. Pratumwal, W. Limtrakaran, S. Muengtaweepongsa, P. Phakdeesan, K. Intharakham, *Whole blood viscosity modelling using power las, Casson, and Carreau Yasuda models interegrated with image scanning U-tube viscometer technique.* Songklanakarin J. Sci. Technol. 39 (2017), no. 5, 625-631

46. J.V.R. Reddy, D. Srikanth, D. Samir, K. Das, *Modelling and simulation of temperature and concentration dispersion in a couple stress nanofluid flow through stenotic tapered arteries*, Eur. Phys. J. Plus. 132 (2017), no. 8, 365.

47. L. H. Madkour, *Vision for life sciences: Interfaces between nanoelcectronic and biological systems.* Glob Drugs. Therap. 2 (2017) no. 4, 1-4.

48. M. Dhange, S. Salgare, K. Das, B. Ebenezer, H. Alemayehu, *Hemodynamic Properties of Blood Flow in an Angled Overlying Stenosed Blood Vessel via Force Field and Gold Nanoparticle Suspension*, Sci. Afr. 28 (2025), e02652.

49. R. Sardar, A.M. Funston, P. Mulvaney et al., *Gold nanoparticles: past, present, and future.* Langmuir. 25 (2009), no. 24, 13840-13851.

50. L. H. Madkour, *Applications of gold nanoparticles in medicine and therapy.* Pharm. Pharmacol. Int. J. 6 (2018), no. 3, 157-174.

S. Salgare
Department of Mathematics,
Sanjay Ghodawat University, Kolhapur, Maharashtra,
India.
E-mail address: shrishail.salgare@mt.sguk.ac.in

and

M. Dhange
Department of Mathematics,
BLDEA's VP Dr. PG Halakatti College of Engineering and Technology, Vijayapur, 586103,
India.
(Affiliated to Visvesvaraya Technological University, Belagavi, Karnataka, India)
E-mail address: math.mallinath@bldeacet.ac.in

and

Bhim Shinde
Department of Mathematics, Kolhapur Institute of Technology's College of Engineering, Kolhapur,
India.
E-mail address: shinde.bhim@kitcoek.in

and

Kusha Chavan
Department of Mathematics, BLDEA's VP Dr. PG Halakatti College of Engineering and Technology, Vijayapur
India.
E-mail address: chavankushal013@gmail.com

and

Nurul Aini Jaafar
Department of Mathematical Sciences, Faculty of Science, Universiti Technologi Malaysia,

Malaysia.
E-mail address: nurulaini.jaafar@utm.my

and

J. C. Misra
Department of Mathematics, Indian Institute of Engineering Science and Technology, Shibpur, India.
E-mail address: misrajc@gmail.com